Journal of Medicinal Chemistry

Article

pubs.acs.org/jmc

# Synthesis and Photodynamic Effect of New Highly Photostable Decacationically Armed [60]- and [70]Fullerene Decaiodide Monoadducts To Target Pathogenic Bacteria and Cancer Cells

Min Wang,[†] Liyi Huang,[‡,§] Sulbha K Sharma,[‡] Seaho Jeon,[†] Sammaiah Thota,[†] Felipe F. Sperandio,[‡,§,∥,⊥] Suhasini Nayka,[‡] Julie Chang,[‡,#] Michael R. Hamblin,*[,‡,§,∞] and Long Y. Chiang*[,†,○]

[†]Department of Chemistry, Institute of Nanoscience and Engineering Technology, University of Massachusetts, Lowell, Massachusetts 01854, United States

[‡]Wellman Center for Photomedicine, Massachusetts General Hospital, Boston, Massachusetts 02114, United States

[§]Department of Dermatology, Harvard Medical School, Boston, Massachusetts 02115, United States

[∥]School of Dentistry, University of Sao Paulo, Sao Paulo 05508-000, Brazil

[⊥]CAPES Foundation, Ministry of Education of Brazil, Brasília DF 70040-020, Brazil

[#]Department of Chemistry, Harvard University, Cambridge, Massachusetts 02138, United States

[∞]Harvard-MIT Division of Health Sciences and Technology, Cambridge, Massachusetts 02139, United States

[○]Department of Laboratory Medicine and Pathobiology, University of Toronto, Toronto, Ontario M5S 1A8, Canada

Supporting Information

**ABSTRACT:** Novel water-soluble decacationically armed $C_{60}$ and $C_{70}$ decaiodide monoadducts, $C_{60}$- and $C_{70}[>M(C_3N_6^+C_3)_2]$, were synthesized, characterized, and applied as photosensitizers and potential nano-PDT agents against pathogenic bacteria and cancer cells. A high number of cationic charges per fullerene cage and H-bonding moieties were designed for rapid binding to the anionic residues displayed on the outer parts of bacterial cell walls. In the presence of a high number of electron-donating iodide anions as parts of quaternary ammonium salts in the arm region, we found that $C_{70}[>M(C_3N_6^+C_3)_2]$ produced more $HO^•$ than $C_{60}[>M(C_3N_6^+C_3)_2]$, in addition to $^1O_2$. This finding offers an explanation of the preferential killing of Gram-positive and Gram-negative bacteria by $C_{60}[>M(C_3N_6^+C_3)_2]$ and $C_{70}[>M(C_3N_6^+C_3)_2]$, respectively. The hypothesis is that $^1O_2$ can diffuse more easily into porous cell walls of Gram-positive bacteria to reach sensitive sites, while the less permeable Gram-negative bacterial cell wall needs the more reactive $HO^•$ to cause real damage.

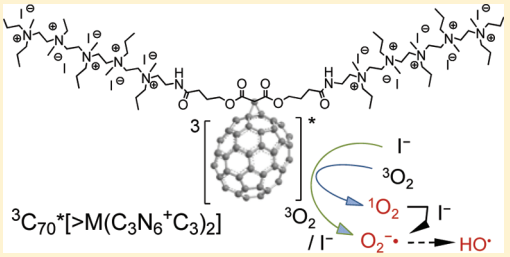


## INTRODUCTION

Photodynamic therapy (PDT)[1−4] employs the combination of nontoxic photosensitizers (PS) with harmless visible to near-IR light to generate highly reactive oxygen species (ROS) such as singlet oxygen ($^1O_2$), superoxide radicals ($O_2^{-•}$), or hydroxyl radicals ($HO^•$) that kill disease-causing cells by a nonspecific attack.[5,6] Increasing prevalence of multiantibiotic drug resistance in multiple classes of pathogens[7,8] contributes to the difficulty in treating the related infectious diseases. Because these pathogens may be deficient in defenses against ROS, especially singlet oxygen and hydroxyl radicals that display a nonspecific high reactivity toward certain critical chemical moieties of the cell, the PDT approach may serve as a promising alternative treatment method for infections and cancer. The nonspecificity nature of PDT also allows its use against a wide range of bacteria, viruses, yeasts, and protozoa by killing these pathogenic agents in the infection.

The reaction mechanism of PDT involves an initial photoexcitation of PS to the singlet excited state upon exposure to a light source, followed by intersystem crossing processes resulting in the formation of a long-lived triplet excited state of PS that can transfer photoenergy to triplet molecular oxygen in the biological system. Accordingly, an effective organic PS should be capable of exhibiting (1) a strong and sharp optical absorption band at the PDT wavelength for a high yield of photoexcitation, (2) a high yield of molecular triplet excited state generation, and (3) effective molecular interactions with the target cell surface to produce ROS in a short distance without undue damage to the surrounding host tissue.

Fullerenes are particularly photostable and manifest little photobleaching compared to many other traditional tetrapyrrole-backbone based PS found in porphyrins and chlorins.[9] Rapid photobleaching characteristics of porphyrin-type PS often disrupt its PDT efficacy after a short period of light illumination mainly because of photodegradation of the

Received: January 16, 2012
Published: April 18, 2012

   dx.doi.org/10.1021/jm3000664 | J. Med. Chem. 2012, 55, 4274−4285

**Scheme 1. Synthetic Pathway for the Preparation of Decacationic $C_{60}[>M(C_3N_6^+C_3)_2]$ 1 and $C_{70}[>M(C_3N_6^+C_3)_2]$ 2**

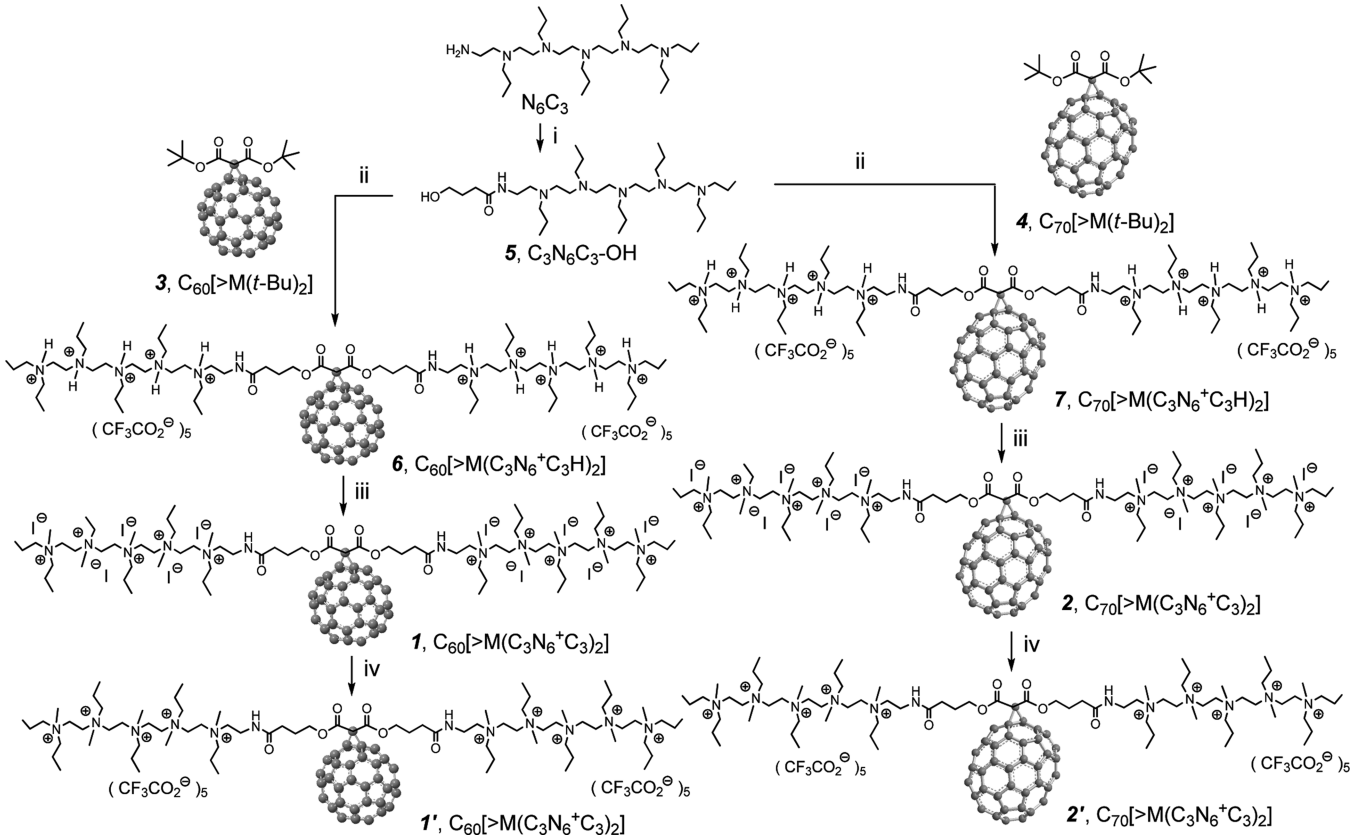


compound and subsequent alteration of its chromophore structure, resulting in the loss of photosensitizing capability. By contrast, a larger number of interlinked aromatic olefinic bonds available on the fullerene cage can tolerate a certain degree of fullerenyl $\pi$-conjugation interruption, induced by the back-attack of singlet oxygen or radical species on the olefin bonds, delaying the loss of their photophysical properties. This chemical nature coupled with a relatively slower reaction rate of $C_{60}$ and $C_{70}$ cages toward ROS than that of porphyrin-type PS leads to a photostability that dramatically extends the length of time they can respond to illumination. It will also allow many more effective catalytic PDT cycles to be carried out with a single application of PS.

Our particular interest is in mediating broad-spectrum PDT killing of pathogenic Gram-positive (e.g., *Staphylococcus aureus*) and Gram-negative (e.g., *Escherichia coli*) bacterial targets. Owing to specific differences in the physiology, cell wall, and cytoplasmic membrane structures between Gram-positive and Gram-negative bacteria,[10−12] it is necessary to significantly revise the functional addends of each fullerene cage for effective targeting selectivity and drug delivery. By taking chemical functional groups and structures of the cell wall into account to maximize potential interaction forces of drugs at the cell surface, the combination of H-bonding and a high number of cationic charges in one molecular compound is beneficial for inducing strong binding. However, synthesis of fullerenyl monoadducts bearing a well-defined high number of cationic charges remains challenging and has rarely been reported.

In this paper, we describe a rational linkage of water-soluble quaternary alkylammonium multisalts and ester amide functional groups into a well-defined decacationic malonate together with an efficient synthetic method for its attachment on either a $C_{60}$ or $C_{70}$ nanocage. The synthesis led to the preparation of new amphiphilic [60]fullerene-based (**1**) or [70]fullerene-based (**2**) nanophotosensitizers, respectively. In these structures, arm moieties each bearing a high number of cationic charges and an amide moiety, capable of inducing the H-bonding in the vicinity of the fullerene cage, are designed for cell targeting. Accordingly, they may allow us to study specifically the feasibility as nano-PDT agents toward both Gram-positive and Gram-negative bacterial species.[2,13] The approach also gives a systematic structure−function relationship of fullerene monoadducts on the influence of their biological activity, aiming to achieve the optimized photodynamic activation and enhancement of the PDT efficiency.

## RESULTS AND DISCUSSION

Surface binding interactions of fullerene derivatives with -D-Ala-D-Ala residues of the bacteria cell wall may be increased by the incorporation of polar moieties on $C_{60}/C_{70}$ capable of inducing multiple H-bondings and static charge interactions with amino acid functional residues. On the basis of this consideration, we applied a malonate precursor arm, as that shown in the structures of $C_{60}[>M(C_3N_6^+C_3)_2]$ **1** and $C_{70}[>M(C_3N_6^+C_3)_2]$ **2** (Scheme 1), to include two esters and two amide moieties for a sufficient number of carbonyl and -NH groups in a short length of ~20 Å for making effective multibinding sites. More importantly, the use of a well-defined water-soluble pentacationic moiety $N_6^+C_3$ at each side of the arm may increase the crucial select-targeting specificity on the bacterial cell wall. Thus, $N_6^+C_3$ becomes a common synthon for the structural modification of PDT nanomedicines. It can be derived from the quarternization of *N,N′,N,N,N,N*-hexapropylhexa(aminoethyl)-amine precursor $N_6C_3$. Attachment of $N_6^+C_3$ to two ester


dx.doi.org/10.1021/jm3000664 | J. Med. Chem. 2012, 55, 4274−4285

moieties of a malonate forms two extended bipolar pentacationic side arms capable of forming strong static-charge binding interactions to anionic carboxylate end-groups of the terminal D-Ala-D-Ala dipeptide of the bacterial cell wall.

Synthetically, large solubility-incompatibility between water-soluble pentacationic intermediate $N_6^+C_3$ side arms and highly hydrophobic fullerene cage incurred much challenge and difficulty in controlling the reaction homogeneity and overall processes for the exclusive monoadduct formation, the efficiency and yield, and the product purification and characterization. Following many attempts using different synthetic routes, we found that the best approach for the preparation of decacationic bis(20-oxo-4,7,10,13,16-pentapropyl-4,7,10,13,16,19-hexaazatricosan-23-yl)[60]fullerenyl malonate methyl quaternary ammonium salt **1** and its $C_{70}$ analogue compound **2** is to begin with a simple well-defined fullerene monoadduct derivatives, such as di(*tert*-butyl)fullerenyl malonates $C_{60}[>M(t\text{-}Bu)_2]$ **3** and $C_{70}[>M(t\text{-}Bu)_2]$ **4**, respectively, capable of undergoing the chemical conversion reaction with $N_6^+C_3$-derived intermediates, as shown in Scheme 1. The alternative approach to synthesize first the water-soluble $N_6^+C_3$-malonate-$N_6^+C_3$ intermediate arm followed by its attachment to a fullerene cage resulted in much complication in the product purification and characterization, even though the same compound was obtained. One potentially plausible synthetic route of using the hydrophobic $N_6C_3$-malonate-$N_6C_3$ intermediate arm was found to be problematic owing to its partial charge-transfer complexation with the [70]fullerene cage.

The structural verification of **4** was made by various spectroscopic techniques, including $^{13}C$ NMR spectrum (Supporting Information) displaying one peak at $\delta$ 162.39 corresponding to the chemical shift of carbonyl carbon and 35 peaks in different intensities (33 peaks each with 2C and two peaks each with 1C) in the region of $\delta$ 125−155 that can be accounted for all 68 fullerenyl $sp^2$ carbons. The data are consistent with a $C_{70}$ monoadduct structure having a $C_s$ symmetrical ellipsoidal structure with a plane of symmetry across the cyclopropane-bridged [6,6] bond. In general, Bingel monoaddition reaction[14] of malonate esters on $C_{70}$ may lead to four regioisomers of methano[70]fullerenes each with a differently bridged [6,6]fullerenyl $sp^3$ bonding location, defined as the $\alpha$-type bonding at the C(1)−C(2), the $\beta$-type bonding at the C(5)−C(6), the $\varepsilon$-type bonding at the C(7)−C(21), and the $\kappa$-type bonding at the C(20)−C(21).[15,16] These regioisomers exhibit a molecular symmetry of $C_s$, $C_{2v}$, $C_1$, and $C_{2v}$, respectively. Chemical reactivity of all these bonding locations was found to be the highest at the most strained region of the cage pole area, giving the order of C(1)−C(2) > C(5)−C(6) > C(7)−C(21) > C(20)−C(21) (lying on the flat equator of the $C_{70}$ spheroid).[17] Therefore, it is reasonable for us to predict the major monomalonate addition product $C_{70}[>M(t\text{-}Bu)_2]$ **4** being the $\alpha$-type analogue. In fact, the $^{13}C$ spectrum of **4** showing the pattern and number of carbon peaks, consistent with the compound having a molecular $C_s$ symmetry, should provide unambiguous support for this structural assignment.

Subsequent facile transesterification reaction of **4** with the well-characterized tertiary amine precursor arm moiety 4-hydroxy-[*N*,*N*′,*N*,*N*,*N*,*N*-hexapropylhexa(aminoethyl)-butanamide **5** ($C_3N_6C_3OH$) was carried out under acidic conditions using trifluoroacetic acid as the catalytic reagent (Scheme 1). The reaction was found to result in the formation of decacationic bis(20-oxo-4,7,10,13,16-pentapropyl-4,7,10,13,16,19-hexaazatricosan-23-yl)[60]fullerenyl malonate, protonated quaternary ammonium trifluoroacetate salt, $C_{70}[>M(C_3N_6^+C_3H)_2]$ **7** in 71% yield. The structure of **7** was verified by various spectroscopic techniques (Supporting Information) including $^{13}C$ NMR spectrum showing two peaks at $\delta$ 170.45 and 165.50 corresponding to the chemical shift of a carbonyl carbon of the amide (−HN−**C**═O) and the ester (−O−**C**═O) moieties, respectively. It also displayed a total of 68 peaks in the region of $\delta$ 125−155, accounting for 68 fullerenyl $sp^2$ carbons. The spectral data clearly indicated a $C_1$ symmetry for compound **7**. As the simple transesterification condition should not complicate the structural configuration of methano[70]fullerene cage moiety, the decrease of molecular symmetry from $C_s$ of **4** may be indicative of strong interactions between flexible hexapropylhexa(aminoethyl)butanamide arms and the $C_{70}$ cage. These interactions may induce a nonsymmetrical environment among cage carbons. It also revealed the likelihood of two pentacationic $C_3N_6C_3$−O− arms to be located at the vicinity of the cage surface, as shown in the cluster form of Figure 1, presumably by the interactive binding of multiple hydrophobic *n*-propyl groups.

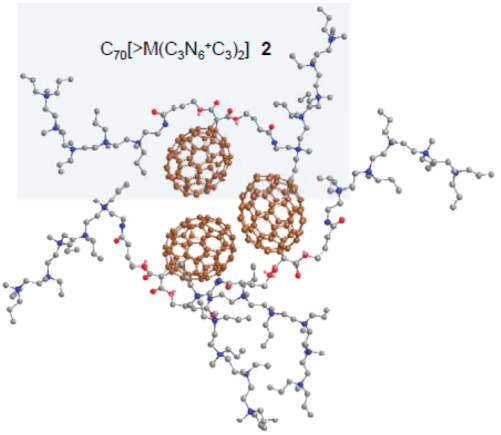


**Figure 1.** Proposed schematic molecular packing of $C_{70}[>M(C_3N_6^+C_3)_2]$ **2** and **2′** by taking the high water solubility of the compound, packing tendency of $C_{70}$ cages, and the analysis of their $^{13}C$ NMR spectra giving the $C_1$ symmetry for the cage moiety into consideration. The drawing was made by using the Chem 3D program for the energy minimization.

Interestingly, we found that the use of $C_{70}$-compatible deuterated solvents, such as $CDCl_3$ and $CS_2$, for enhancing the detectability of [70]fullerenyl carbon peak signals has led to the full suppression of pentacationic arm moieties in the spectrum. In contrast, the application of water-compatible deuterated solvents, such as $D_2O$ and DMF-$d_7$, significantly reduced the signal intensity of [70]fullerenyl carbon peaks, likely owing to the cage aggregation.

Conversion of compound **7** to decacationic bis(20-oxo-4,7,10,13,16-pentapropyl-4,7,10,13,16,19-hexaazatricosan-23-yl)[70]fullerenyl malonate methyl quaternary ammonium salt, $C_{70}[>M(C_3N_6^+C_3)_2]$ **2**, was accompanied by multiple iodide anions. The infrared spectrum of **2** clearly showed four sharp characteristic bands at 794.33, 723.08, 578.72, and 530.19 $cm^{-1}$ corresponding to the absorption of a $C_{70}$ half-cage, revealing no bismalonate adduct formation (with an additional malonate addend attached at the $\alpha$-bond of the opposite pole). Unexpectedly, we were not able to detect any fullerenyl $sp^2$ carbon signals in the $^{13}C$ NMR spectrum of **2** under various


dx.doi.org/10.1021/jm3000664 | J. Med. Chem. 2012, 55, 4274−4285

deuterated solvent mixtures. However, these carbon signals reappeared when all iodide anions were replaced by trifluoroacetate anions, leading to the corresponding salt **2′**. Accordingly, the $^{13}C$ NMR spectrum of **2′** displayed a peak at $\delta$ 170.45 corresponding to the chemical shift of an amide carbonyl carbon (−HN−**C**═O), similar to that of **7**. It also displayed a total of 68 peaks in the region of $\delta$ 125−155, accounting for 68 fullerenyl $sp^2$ carbons, indicating a similar $C_1$ symmetry as that of the compound **7**. The observation led to our assumption of the possibility of reversible partial electron-transfer from the iodide ($I^-$) donors to $C_{70}$ cages, forming a low degree of radicalized cage moieties that significantly reduced the resolution of $^{13}C$ signals.

The mass spectroscopic data collection of $C_{70}[>M(C_3N_6^+C_3)_2]$ was proven to be difficult because of its polycationic nature and facile fragmentations occurring at the conjunction of the $C_{70}$ cage and the decacationic malonate arm, giving mainly the highly detectable $C_{70}$ ion mass at $m/z$ 841, as displayed in MALDI-TOF mass spectra (Supporting Information). Fortunately, we are able to acquire several spectra in the high mass region showing the molecular ion mass ($M^+$) at $m/z$ 3340 in low intensity accompanied by several identifiable fragmentation ion mass peaks at $m/z$ 1355, 1584, 1654, 1682, 1753, 2043, and 2079. By variation of applied laser intensity, spectra containing many ion mass peaks in significant signal intensity in the medium mass region can be obtained. Structural elucidation of these ion fragments (Supporting Information) in these two spectra allowed us to conclude (1) a clear monoadduct structure of **2** by the sole detection of an ion fragment mass of $C_{70}(-CH_3)^+$ at $m/z$ 855 without the corresponding ion fragment mass of the bisadduct $C_{70}(-CH_3)(>CH_2)^+$ at $m/z$ 869, (2) a facile process of nearly full dequaternization of **2** under MALDI-MS conditions giving mostly detectable monocationic mass fragments, and (3) the bond cleavage of *n*-propyl group on the nitrogen atom is faster than that of the methyl group and the main chain moiety. These data strongly support the molecular mass of **2** as a $(C_3N_6^+C_3)_2$-malonate-$C_{70}$ structure with many consistent $(C_3N_6C_n)_2$-malonate-$C_{70}$ ($C_n$: methyl or *n*-propyl group) fragments.

The molecular aggregation characteristics of amphiphilic nanostructures **1** and **2** in water were investigated under the preparation condition in close resemblance to that used in the in vitro PDT studies. Typically, the sample was dissolved in DMA under ultrasonication for a period of ∼5.0 min, giving a master solution at 2.0 mM. A portion of this solution was then diluted by $H_2O$ to predetermined concentrations of 1.0, 10, and 100 $\mu$M for transmission electron microscopy (TEM) measurements. As a result, TEM micrographs of $C_{60}[>M(C_3N_6^+C_3)_2]$ displayed no obvious bilayered fullerosome[18−20] formation at either 1.0 or 10 $\mu$M. A sporadic formation of fullerosome vesicles each in a larger particle diameter of 60−100 nm was observed at a higher concentration of 100 $\mu$M. In the case of $C_{70}[>M(C_3N_6^+C_3)_2]$, a similar observation of no clearly detectable bilayered fullerosome nanovesicles was found at all concentrations of 1.0, 10, and 100 $\mu$M. There was only a small quantity of irregularly shaped nanospherical particles of **2** found at 10 and 100 $\mu$M. This implied that the hydrophilic strength of two pentacationic arms overwhelm the hydrophobic character of $C_{60}$ and $C_{70}$ cages, leading to high water solubility of **1** and **2** with much suppression of their tendency to form sizable particles under PDT experimental conditions. In the light of a slightly higher ability of the $C_{70}$ moiety, with 10 more carbon atoms in one cage, to give molecular cluster formation compared with $C_{60}$, we proposed a likely molecular cluster packing configuration of **2** and **2′** in water, as shown in Figure 1. It includes unsymmetrical hydrophobic malonate ester arm moiety interactions with the $C_{70}$ cage that induce the loss of molecular cage symmetry observed in its $^{13}C$ NMR spectrum. Partial blocking of the cage surface by the arms allows only a very limit number of hydrophobic cages to undergo irregular coalescence into a nanosphere in $H_2O$.

The light-induced PDT efficiency can be correlated partially to optical absorption extinction coefficients of the PS in the wavelength range applied. Accordingly, we studied UV−vis spectra of $C_{60}[>M(C_3N_6^+C_3)_2]$ and $C_{70}[>M(C_3N_6^+C_3)_2]$ in DMA at $1.0 \times 10^{-5}$ M, as shown in Figure 2A, in comparison

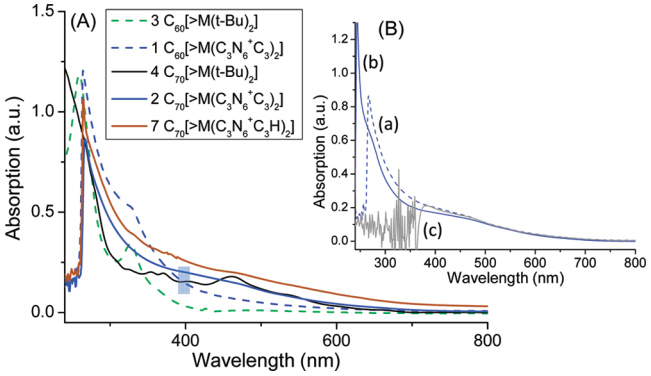


**Figure 2.** UV−vis spectra of (A) $C_{60}[>M(t\text{-Bu})_2]$ **3** in $CHCl_3$, $C_{60}[>M(C_3N_6^+C_3)_2]$ **1** in DMAc, $C_{70}[>M(t\text{-Bu})_2]$ **4** in $CHCl_3$, $C_{70}[>M(C_3N_6^+C_3)_2]$ **2** in DMAc, and $C_{70}[>M(C_3N_6^+C_3H)_2]$ **7** in DMAc and (B) $C_{70}[>M(C_3N_6^+C_3)_2]$ **2** in (a) DMAc, (b) DMAc−$H_2O$ (1:19), and (c) DMAc−$CHCl_3$−$CS_2$ (1:1:2). The concentration of all samples is $1.0 \times 10^{-5}$ M.

with the parent monoadducts $C_{60}[>M(t\text{-Bu})_2]$ **3** and $C_{70}[>M(t\text{-Bu})_2]$ **4** in $CHCl_3$. Interestingly, the optical absorption profile of **4** showing peaks with the maxima ($\lambda_{max}$) located at 355, 370, 403, 462, and 539 (shoulder band) nm matches well with those reported for the $\alpha$-type $C_{70}$ monoadducts,[21,22] which provided further confirmation of our structural assignment of **4**. Upon the structural conversion of **4** with decacationic di($C_3N_6C_3$-O)-malonate arm, the intensity of absorption of $C_{70}[>M(C_3N_6^+C_3)_2]$ increases at wavelengths of <450 nm with the disapperance of all characteristic peaks of the monoadduct **4** into a featureless curve. Since the cage moiety was not modified from **4**, the difference may imply the occurrence of cage cluster formation, consistent with that proposed in Figure 1. The change leads to a higher total visible absorption of **2** compared with the $C_{60}$ analogue **1** in a ratio of 1.99 ($\varepsilon_2/\varepsilon_1$) over 400−700 nm (Figure 2A). However, an opposite relationship was found in the UVA region (320−400 nm), giving a $\varepsilon_2/\varepsilon_1$ ratio of 0.79, indicating a stronger optical absorption of $C_{60}$ monoadduct cage in this wavelength range. It is also interesting to note the higher $\varepsilon$ for the protonated quaternary ammonium trifluoroacetate salt, $C_{70}[>M(C_3N_6^+C_3H)_2]$ **7**, compared with that for **2** over all wavelengths (300−800 nm). To correlate the light absorption efficiency of **2** under PDT experimental conditions, we compared its visible spectrum profile taken in DMAc−$H_2O$ (1:19) to that in DMA (curves a and b of Figure 2B) and found a nearly identical $\varepsilon$ over the range 400−700 nm. Photostability of $C_{60}[>M(C_3N_6^+C_3)_2]$ and $C_{70}[>M(C_3N_6^+C_3)_2]$ in aqueous solution


dx.doi.org/10.1021/jm3000664 | J. Med. Chem. 2012, 55, 4274−4285

was evaluated under constant irradiation using a LED light source equipped with a fiber optical lens (200 mW/cm$^2$ at 400 ± 5 nm) over a period of 5.0 h. Consequently, high retention of a UV−vis absorption profile of fullerene derivatives was observed.

**ROS Probe Experiments.** Illumination of $C_{60}$ or $C_{70}$ monoadduct derivatives with visible or UVA light promotes its transition to a long-lived trriplet excited state via intersystem crosing processes and subsequent intermolecular energy transfer to the molecular oxygen, yielding a highly reactive singlet oxygen ($^1O_2$) in type II reactions.[23] In the presence of physiological concentration of reductants such as NADH, more reactive ROS species, such as superoxide anion ($O_2^{-\bullet}$) and hydroxyl radical (HO$^\bullet$), may be produced in polar solvent and water.[24] In this study, a comparative singlet oxygen production efficiency study of compounds **1** and **2** in DMSO−$H_2O$ (1:520, 1.0 × 10$^{-6}$ M) was carried out with many incremental exposures of the sample to a Uvitron visible-enhanced lamp (200 W, 250−600 nm with $\lambda_{max}$ at 420 nm) in an exposure interval period of 5.0 s (the light dose measured to be ∼5.0 mJ/cm$^2$ per period) followed by the fluorescence emission measurement of the probe. For highly efficient in situ selective trapping of singlet oxygen, we applied water-compatible 9,10-anthracenediyl-bis(methylene)dimalonic acid (ABMA, 8.0 × 10$^{-6}$ M) as a fluorescent probe which exhibits the emission maximum at 429 nm. The corresponding most effective excitation wavelengths were found to be 379 and 400 nm. Accordingly, the later one closer to the visible range was used. At this wavelength, the optical absorption extinction coefficient of **2** is slightly higher than that of **1**, as shown by the blue mark in Figure 2A. The chemical trapping of $^1O_2$ by highly fluorescent ABMA leads to the formation of nonfluorescent 9,10-endoperoxide product. The conversion allows us to follow the loss of fluorescence emission intensity at 429 nm for its correlation to the proportional quantity of $^1O_2$ produced because of the high kinetic rate constant of the trapping reaction in aqueous medium,[25] assuming the internal decay of $^1O_2$ in the solvent system is identical for both experiments of **1** and **2**. As a result, we observed a slightly higher $^1O_2$ production rate of $C_{60}[>M(C_3N_6^+C_3)_2]$, even though the difference is not statistically significant, as shown in Figure 3a. The use of a lower irradiation dose for a similar measurement directly in the UV−vis−NIR spectrometer, operating at $\lambda_{ex}$ = 400 nm (single wavelength excitation) with the monochromator, gave a much slower production rate of $^1O_2$ for both cases that displayed a clearly higher rate for $C_{60}[>M(C_3N_6^+C_3)_2]$ at this excitation wavelength (Figure 3b).

A similar trend was also confirmed by using $^1O_2$ probe singlet oxygen sensor green (SOG) reagent. Upon the trapping of $^1O_2$ by the anthracene moiety of SOG, the resulting 9,10-endoperoxide-linked fluorescein product SOG-EP is highly green fluorescent (excitation/emission maxima of ∼504/525 nm) that can be used for the correlation of the relative $^1O_2$ quantity produced. It is worthwhile to mention that the SOG probe chemistry is potentially more complicated than the statement above because of the fact that both SOG and SOG-EP are capable of sensitizing $^1O_2$ production and undergoing photobleaching processes themselves, resembling those of fluorescein derivatives.[26] This complication can be lessened by using blue light for fullerene excitation that is not absorbed by the probe. However, if we assume that the amount of the additional $^1O_2$ molecules derived from SOG and SOG-EP and the photobleaching rate are nearly identical among experiments

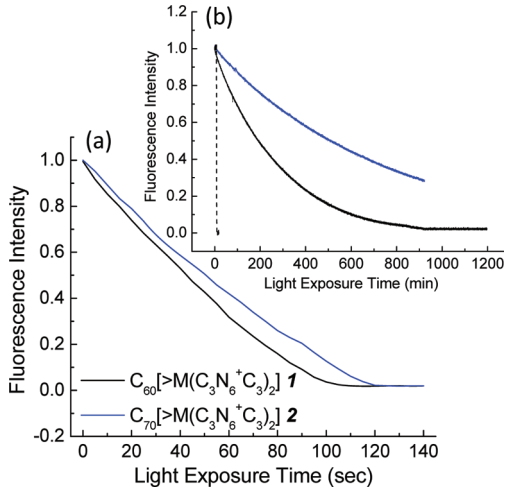


**Figure 3.** Comparison of singlet oxygen production efficiency of compounds **1** and **2** in DMSO−$H_2O$ (1:520, 1.0 × 10$^{-6}$ M), using anthracene tetracarboxylic acid ABMA (8.0 × 10$^{-6}$ M) as the fluorescent $^1O_2$-trapping agent at $\lambda_{ex}$ 400 nm and $\lambda_{em}$ 429 nm for detection with an irradiation source of (a) Uvitron lamp (200 W) and (b) spectrometer lamp/monchromator operated with a single wavelength at $\lambda_{ex}$ 400 nm.

under the same conditions, the fluorescence emission intensity of SOG-EP detected will still be valuable for a relative comparison. Accordingly, Figure 4a shows the results from the SOG-based fluorescence probe assay experiments of **1** and **2** in 96-well black-sided plates under incremental irradiation with a blue LED light source (415 ± 15 nm) under the total fluence intensity range of 0−6.0 J/cm$^2$. It is evident that $C_{60}[>M(C_3N_6^+C_3)_2]$ gave a significantly higher rate of $^1O_2$ detected than $C_{70}[>M(C_3N_6^+C_3)_2]$. The marked difference in the $^1O_2$ generation rate of **1** and **2** between the data of Figure 3 (without PBS) and Figure 4a (with PBS) led to our consideration of the potential involvement of type I photoreaction processes in electrolyte solution giving reactive radical species in the latter experimental conditions.

Indeed, under similar experimental procedures relevant to PDT as those used for the data collection of Figure 4a but with the application of the fluorescent probe of 3′-*p*-(hydroxyphenyl)fluorescein[27] (HPF), a reverse relationship was observed with higher fluorescence emission intensity of fluorescein for $C_{70}[>M(C_3N_6^+C_3)_2]$ than for $C_{60}[>M(C_3N_6^+C_3)_2]$ under the total fluence intensity range of 0−5.0 J/cm$^2$, as shown in Figure 4b. Since the HPF probe is an essential tool for the selective detection of HO$^\bullet$ and peroxynitrite, via quinone formation detached from the fluorescein moiety (excitation/emission maxima of ∼490/515 nm), with the detection sensitivity reported to be roughly 145- and 90-fold higher for HO$^\bullet$ than for $^1O_2$ and $O_2^{-\bullet}$, respectively,[27] the measured fluorescence intensity can be correlated roughly to the yield of hydroxyl radicals produced. Besides, $O_2^{-\bullet}$ is the precusor species to the formation of HO$^\bullet$. Directly monitoring the presence of HO$^\bullet$ will also serve to confirm superoxide radical formation, i.e., higher yield for $C_{70}[>M(C_3N_6^+C_3)_2]$ than for $C_{60}[>M(C_3N_6^+C_3)_2]$.

It is well-recognized that $^1O_2$ can give rise to several other types of ROS, including $O_2^{-\bullet}$, $H_2O_2$, and HO$^\bullet$, in a sequential reaction with iodide anion ($I^-$),[28] In this case, the yield of $O_2^{-\bullet}$ or HO$^\bullet$ should be proportional to the quantity of $^1O_2$. Therefore, our observation of a higher $^1O_2$ production yield of


dx.doi.org/10.1021/jm3000664 | J. Med. Chem. 2012, 55, 4274−4285

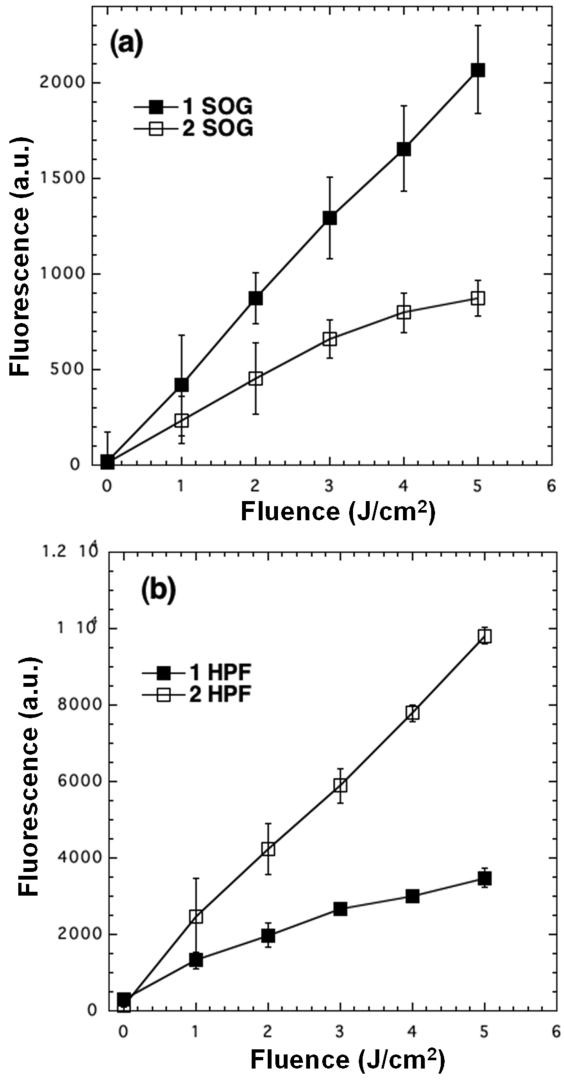


**Figure 4.** Activation of fluorescence probes for detecting the ROS generation by **1** and **2** (5.0 $\mu$M in each well) using different fluorescent probes (a) SOG (5.0 $\mu$M) and (b) HPF (5.0 $\mu$M), followed by delivery of the stated fluence of blue light.

$C_{60}[>M(C_3N_6^+C_3)_2]$ in PBS solution (Figure 4a) giving a lower production yield of radical species (Figure 4b) revealed no direct correlation of $^1O_2$ to $O_2^{-\bullet}$ or HO$^\bullet$ yields, or the latter species may not be derived directly from the former one in these experiments. In contrast, they may be in a competitive production process with each other in either the triplet energy-transfer (type II) or electron-transfer (type I) mechanism involving the electron-donating iodide anion ($I^-$) and the electron-accepting fullerene cage. This mechanistic path can be realized by the facile photoexcitation of $C_{60}/C_{70}$ cages to their singlet excited state followed by quantitative intersystem crossing to their corresponding excited triplet transient states, $^3C_{60}*[>M(C_3N_6^+C_3)_2]$ and $^3C_{70}*[>M(C_3N_6^+C_3)_2]$. Apparently, the latter molecule exhibited a higher electron-accepting capability to allow electron transfer from the iodide anion, leading to the formation of $C_{70}^{-\bullet}[>M(C_3N_6^+C_3)_2]$ prior to the further transfer this electron to $O_2$ that gave a higher yield of $O_2^{-\bullet}$ and thus HO$^\bullet$.

**Antimicrobial Effect of Fullerene-Mediated PDT.** Two highly water-soluble decacationic fullerenes **1** and **2** were first applied for comparison in the PDT-killing of the Gram-positive *S. aureus*. In general, it is known that Gram-positive bacteria are more sensitive and susceptible to PDT destruction than Gram-negative bacteria. This allowed us to use a lower concentration (up to 10 $\mu$M) of fullerene derivatives for *S. aureus* killing than that (up to 100 $\mu$M) needed for effective *E. coli* killing. Our previous PDT experiments have indicated a fast binding process of PS to microbial cells.[29] Thus, a short incubation time of 30 min was applied for both species. As shown in Figure 5,

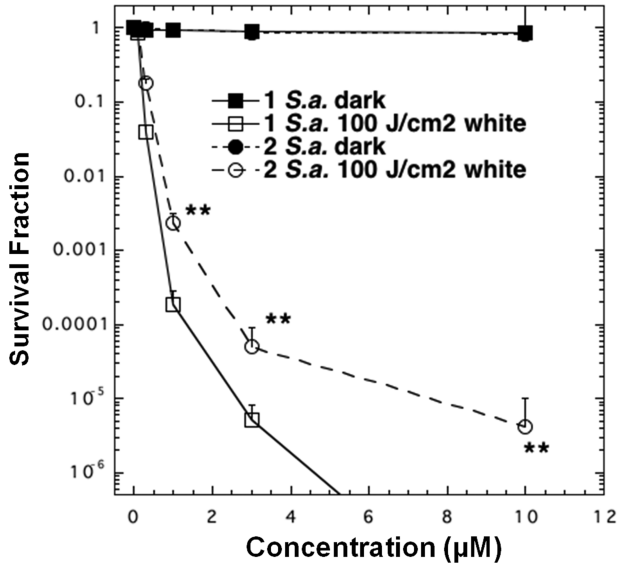


**Figure 5.** PDT killing of Gram-positive bacteria *S. aureus*. Bacteria [$10^8$ cells/mL] were incubated with stated concentration of $C_{60}[>M(C_3N_6^+C_3)_2]$ **1** or $C_{70}[>M(C_3N_6^+C_3)_2]$ **2** for 30 min followed by delivery or not of 100 J/cm$^2$ of white light: (**) $p < 0.01$.

neither decacationic fullerene derivative **1** nor **2** gave any detectable toxicity to both bacteria in the dark at a concentration up to 10 $\mu$M. A pronounced PDT effect was observed after illumination on the **1**/**2**-incubated cells using a broad-band white light source with total fluence intensity of 100 J/cm$^2$ with a sharp cytotoxicity trend even at a low fullerene concentration of 1.0 $\mu$M, giving 3 log killing for $C_{60}[>M(C_3N_6^+C_3)_2]$ and 2 log killing for $C_{70}[>M(C_3N_6^+C_3)_2]$. As the administered dose increased to 3.0 $\mu$M, a 5 log killing effectiveness was observed for the compound **1** and a corresponding 3 log for the compound **2**. Interestingly, $C_{60}[>M(C_3N_6^+C_3)_2]$ was able to eradicate the cells at concentrations higher than 3.0 $\mu$M. In the case of $C_{70}[>M(C_3N_6^+C_3)_2]$, a 5 log effective killing was achieved at 10 $\mu$M. Two killing curves of **1** and **2** were significantly different from each other ($p < 0.01$).

In the PDT experiments against *E. coli*, the need to use 8 times higher concentrations of fullerene drugs led to the observation of some dark toxicity (1−2 log) at the higher concentrations of 60 and 80 $\mu$M. Surprisingly, the order of PDT effectiveness of these two fullerene drugs was opposite to that seen with *S. aureus*. In this case, $C_{70}[>M(C_3N_6^+C_3)_2]$ was most effective for *E. coli* killing with 3 log at 40 $\mu$M and 5 log at 60 $\mu$M and for eradicating the cells at 80 $\mu$M, as shown in Figure 6. On the other hand, $C_{60}[>M(C_3N_6^+C_3)_2]$ only killed 1 log at 40 $\mu$M, 2 log at 60 $\mu$M, and 3 log at 80 $\mu$M. These two curves were significantly different ($p < 0.01$).

**Anticancer Effect of Fullerene-Mediated PDT.** A longer incubation period of 24 h was applied for the experiments with


dx.doi.org/10.1021/jm3000664 | J. Med. Chem. 2012, 55, 4274−4285

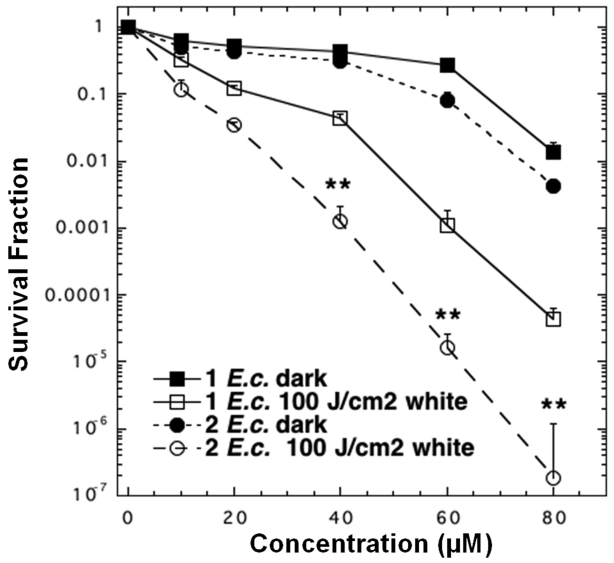


**Figure 6.** PDT killing of Gram-negative bacteria *E. coli*. Bacteria [$10^8$ cells/mL] were incubated with stated concentration of **1** or **2** for 30 min followed by delivery or not of 100 J/cm$^2$ of white light: (**) $p < 0.01$.

cancer cells owing to their relatively slow process to uptake fullerene derivatives. Furthermore as it appears that cancer cells are more sensitive to the dark toxicity effects of both fullerene derivatives and DMA organic solvent, we kept the concentration to a single low value of 2.0 $\mu$M. The irradiation was made by a white light source (400–700 nm) delivered at an intensity of 100 mW/cm$^2$ with a variable fluence dose of 0, 10, 20, 40, and 80 J/cm$^2$ for giving a demonstration of a light-dose dependence of cell killing. As depicted in Figure 7, $C_{70}$[>M-($C_3N_6^+C_3$)$_2$] was apparently more effective at cancer-cell killing than $C_{60}$[>M($C_3N_6^+C_3$)$_2$], with 1 log of cells killing at 40 J/cm$^2$ and 2 log at 80 J/cm$^2$. Since the MTT assay cannot reliably measure more than 2 log of killing, the latter light-dose

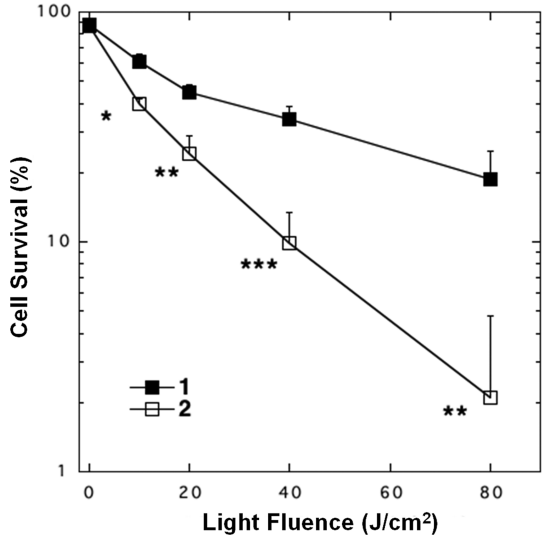


**Figure 7.** PDT killing of human cancer cells. HeLa cells were incubated with 2.0 $\mu$M $C_{60}$[>M($C_3N_6^+C_3$)$_2$] **1** or $C_{70}$[>M($C_3N_6^+C_3$)$_2$] **2** for 24 h, followed by delivery of stated fluence of white light. The cells were then returned to incubator for 24 h. The MTT assay was then carried out: (*) $p < 0.05$; (**) $p < 0.01$; (***) $p < 0.001$.

effectiveness is equivalent to eradication. By contrast, the fullerene drug **1** killed less than 1 log at all fluences up to 80 J/cm$^2$. These two curves were significantly different ($p < 0.05$–0.001).

**Discussion of PDT Results.** The data showed interesting differences between the photoactivity of decacationic fullerene compounds that differ only in the number of carbon atoms in the fullerene cage. The decacationic arms attached to these fullerenes served to give the molecules rapid binding to the anionic residues displayed on the outer parts of bacterial cell walls. The large number of ionic groups attached to the fullerene also provided enhanced water solubility, which is a necessary requirement for biological activity. Even though these fullerenes displayed a rapid ability to photoinactivate bacteria, they were also efficient in mediating the PDT killing of cancer cells, although a longer incubation time was needed. A large molecular weight of these fullerenes (around 3300) means that they are too large to diffuse through the plasma membrane of mammalian cells, which is a rapid process, and are therefore taken up by the slower process of adsorptive endocytosis. The differences in effectiveness we found between $C_{60}$ and $C_{70}$ was interesting. For Gram-positive bacteria $C_{60}$[>M($C_3N_6^+C_3$)$_2$] was better at photokilling than $C_{70}$[>M($C_3N_6^+C_3$)$_2$], while for Gram-negative bacteria and for cancer cells the opposite was the case, in that $C_{70}$[>M($C_3N_6^+C_3$)$_2$] was better at photokilling than $C_{60}$[>M($C_3N_6^+C_3$)$_2$]. We have previously reported[30] that type II reactive oxygen species (ROS), i.e., singlet oxygen, $^1O_2$, are better at killing Gram-positive bacteria than type I ROS, i.e., hydroxyl radicals, HO$^\bullet$, while the reverse is true for Gram-negative bacteria (HO$^\bullet$ is better at killing than $^1O_2$). Therefore, we decided to test the type of ROS (HO$^\bullet$ or $^1O_2$) produced when **1** and **2** were illuminated in simple PBS solution. To do this, it was necessary to employ blue light to excite the fullerene, because if white light was used, the light alone would activate the probe to some extent through the green absorption peak. The results demonstrated that $C_{60}$[>M($C_3N_6^+C_3$)$_2$] produced more $^1O_2$ while $C_{70}$[>M($C_3N_6^+C_3$)$_2$] produced more HO$^\bullet$. This finding offers an explanation of the preferential killing of Gram-positive bacteria by **1** and the preferential killing of Gram-negative bacteria by **2**. The hypothesis is that $^1O_2$ can diffuse more easily into porous cell walls of Gram-positive bacteria to reach sensitive sites, while the less permeable Gram-negative bacterial cell wall needs the more reactive HO$^\bullet$ to cause real damage[31,32] It has not been reported whether HO$^\bullet$ or $^1O_2$ is more efficient in killing cancer cells, but our data would suggest that HO$^\bullet$ may be more effective in this case as well.

## ■ CONCLUSION

A novel water-soluble decacationic armed $C_{70}$ monoadduct decaiodide $C_{70}$[>M($C_3N_6^+C_3$)$_2$] was synthesized, characterized, and applied as a PS and potential nano-PDT agent against pathological bacteria and cancer cells. The arm structure was designed to include a large number of cationic charges per $C_{70}$, and H-bonding moieties were designed for rapid binding to the anionic residues displayed on the outer parts of bacterial cell walls and high water-solubility. The use of propyl groups on quaternary ammonium salt moieties was to provide an interaction balance between the arm moieties and the cage in the presence of water. These structural characterisatics were found to overwhelm the hydrophobicity of the fullerene cage moiety that largely prohibited a sizable cage aggregation in water.

In the presence of a high number of electron-donating iodide anions as parts of quaternary ammonium salts in the arm region, we found that $C_{70}[>M(C_3N_6^+C_3)_2]$ produced more $HO^\bullet$ than $C_{60}[>M(C_3N_6^+C_3)_2]$, in addition to $^1O_2$. Both ROS were detected using several fluorescence probes. This finding offers an explanation of the preferential killing of Gram-positive and Gram-negative bacteria by $C_{60}[>M(C_3N_6^+C_3)_2]$ and $C_{70}[>M(C_3N_6^+C_3)_2]$, respectively. The data are consistent with the hypothesis that $^1O_2$ can diffuse more easily into porous cell walls of Gram-positive bacteria to reach sensitive sites, while the less permeable Gram-negative bacterial cell wall needs the more reactive $HO^\bullet$ to cause real damage. Since the production rate of $^1O_2$ was detected in a similar range for **1** and **2** in the absence of PBS, the differences shown in the presence of PBS electrolyte salts led to our suggestion that the observed production of $HO^\bullet$ may arise partially from the photoinduced electron-transfer (type I) mechanism involving the electron-donating iodide anions ($I^-$) and the fullerene cages at their excited triplet transient states, $^3C_{60}*[>M(C_3N_6^+C_3)_2]$ and $^3C_{70}*[>M(C_3N_6^+C_3)_2]$, having different electron-accepting strength. The presence of electrolyte salts makes the ion exchange and $I^-$ dissociation possible and increases the efficiency of electron transport that forms the corresponding $C_{60}^{-\bullet}[>M(C_3N_6^+C_3)_2]$ and $C_{70}^{-\bullet}[>M(C_3N_6^+C_3)_2]$, respectively, as the source for the $O_2^{-\bullet}$ and the derived ROS radicals generation.

We previously reported[33] that antimicrobial PDT using a cationic functionalized fullerene and white light for mice with wounds that were heavily contaminated with bacteria could prevent the death of mice due to the development of sepsis. The possible clinical application of fullerenes as PDT agents is to some degree limited by the need to use shorter wavelength light for excitation, but we have also recently reported[34] that this drawback can actually be an advantage when shorter penetration into tissue is desired. The temporal selectivity (short times give binding to bacteria, while long times allow uptake into mammalian cells) suggests that the same agents could be used to treat both infections and cancer.[35] When fullerene mediated PDT is used with a long incubation time, it can kill multiple types of cancer cells, including head, neck, breast, and esophageal cancer, that respond poorly to alternative cancer therapies.

## EXPERIMENTAL SECTION

**Materials.** Reagents γ-butyrolactone (GBL), $BF_3{\cdot}Et_2O$, triethylamine, 1,8-diazabicyclo[5,4,0]undec-7-ene (DBU), carbon tetrabromide ($CBr_4$), trifluoroacetic acid, potassium carbonate, and iodomethane were purchased from Aldrich Chemicals and used without further purification. Di-*tert*-butyl malonate was purchased from Tokyo Chemical Industry Co., Ltd. A $C_{60}$ sample with a purity of 99.0% and a $C_{70}$ sample with a purity of 98.0% were purchased from either Nano-C, Inc. or Term USA, Inc. 9,10-Anthracenediyl-bis(methylene)-dimalonic acid (ABMA) was either purchased from Santa Cruz Biotechnology, Inc. or synthesized according to the literature procedure.[36] Sodium sulfate was employed as a drying agent. Solvents were routinely distilled before use. Singlet oxygen sensor green (SOG) and 3′-*p*-(hydroxyphenyl)fluorescein (HPF) were obtained from Invitrogen, Ltd. as solutions in either methanol (SOG) or dimethylformamide (HPF).

**Spectroscopic Measurements.** Infrared spectra were recorded as KBr pellets on a Thermo Nicolet Avatar 370 FT-IR spectrometer. $^1H$ NMR and $^{13}C$ NMR spectra were recorded on a Bruker Avance Spectrospin-500 spectrometer. UV−vis spectra were recorded on a Perkin-Elmer Lambda 750 UV−vis−NIR spectrometer. MALDI mass spectra were recorded on a WATERS Micromass MALDI-TOF mass spectrometer. Elemental analysis was taken by Galbraith Laboratories, Inc. These spectroscopic methods were applied for all compounds synthesized in conjunction with elemental analysis of some compounds to confirm that the purity of samples was at least ≥95%.

**Synthesis of Di(*tert*-butyl)[70]fullerenyl Malonate, $C_{70}[>M(t\text{-}Bu)_2]$ 4.** Finely divided [70]fullerene (2.3 g, 2.7 mmol) was taken into a round-bottom flask. Anhydrous toluene (1.6 L) was added under nitrogen. The solution was stirred for 12 h at ambient temperature to ensure complete dissolution of $C_{70}$. To the resulting wine-colored solution was added carbon tetrabromide (0.56 g, 1.68 mmol) followed by a solution of di-*tert*-butyl malonate (0.3 g, 1.39 mmol) in anhydrous toluene (100 mL). The solution was stirred for an additional 30 min, and to it was slowly added 1.8-diazabicyclo[5.4.0]-undec-7-ene (DBU, 0.52 g, 3.4 mmol) over a period of 15 min. The color of the solution slowly turned brown in 8.0 h. The solution was then concentrated on a rotary evaporator to roughly 50 mL. Upon the addition of methanol to this concentrated solution, the crude product was precipitated as a brown solid which was collected via centrifugation. Purification of di(*tert*-butyl)[70]fullerenyl malonate, $C_{70}[>M(t\text{-}Bu)_2]$ **4**, was made by column chromatography (silica gel using toluene/hexane (1:1, v/v) as eluent) to afford a brown solid in a yield of 65.0% (0.95 g). Spectroscopic data of the compound **4**: MALDI-TOF-MS (sinapic acid as the matrix, rel intensity) *m*/*z* 841 ($C_{70}H^+$, 56%), 855 ($C_{70}CH_3^+$, 100%), 866 (28%), 882 (13%), 900 (79%), 913 (27%), 926 (28%), 944 (11%), 1023 (8%), 1055 ($MH^+$, 5%), and 1056 (8%); FT-IR (KBr) $\nu_{max}$ 3444 (vs, water peak), 2997 (w), 2974 (m, −C−H stretching), 2923 (m, −C−H stretching), 2849 (w), 1741 (vs, malonyl ester −C═O), 1720 (s, malonyl ester −C═O), 1647 (m), 1468 (w), 1451 (m, antisymmetric deformations of $-CH_3$), 1427 (s), 1391 (m), 1366 (s, symmetric deformations of $CH_3$), 1308 (w), 1273 (s), 1250 (s, asymmetric stretching of −C−C(═O)-O−), 1150 (vs, −C−O−*t*-Bu stretching and C($C_{60}$)−C−C(═O)− deformations), 1093 (s), 1025 (w), 954 (w), 877 (w), 843 (m), 794 (m, $C_{70}$), 752 (m), 671 (m, $C_{70}$), 649 (w), 640 (m), 577 (s, $C_{70}$), 532 (s, $C_{70}$), and 458 (m, $C_{70}$) $cm^{-1}$; UV−vis ($CHCl_3$, cutoff at 245 nm, $1.0 \times 10^{-5}$ M) $\lambda_{max}$ 322, 355, 370, 403, 462, and 539 (shoulder band) nm; $^1H$ NMR (500 MHz, $CDCl_3$, ppm) δ 1.68 (s, 18H); $^{13}C$ NMR (500 MHz, $CDCl_3$−$CS_2$, ppm) δ 162.39 (−C═O), 155.41 (2C), 151.57 (2C), 151.32 (2C), 150.86 (2C), 150.74 (2C), 149.48 (2C), 149.39 (2C), 149.21 (2C), 148.76 (2C), 148.71 (2C), 148.68 (2C), 148.62 (2C), 147.78 (2C), 147.71 (2C), 147.46 (2C), 147.15 (2C), 146.60, 146.09 (2C), 146.05 (2C), 145.06 (2C), 145.01, 144.10 (2C), 144.00 (2C), 143.63 (2C), 143.36 (2C), 142.93 (2C), 142.24 (2C), 141.81 (2C), 140.77 (2C), 137.30 (2C), 133.74 (2C), 132.98 (2C), 131.05 (2C), 130.97 (2C), 130.95 (2C), 84.86 (2C), 28.25 (6C), indicating a molecular $C_s$ symmetry for **4**.

A similar procedure was applied for the preparation of di(*tert*-butyl)[60]fullerenyl malonate, $C_{60}[>M(t\text{-}Bu)_2]$ **3**, in a yield of 62.0%. Spectroscopic data: MALDI-TOF-MS (sinapic acid as the matrix, rel intensity) *m*/*z* 721 ($C_{60}H^+$, 70%), 734 ($C_{60}CH_2^+$, 100%), 747 ($C_{60}CHCH_2^+$, 37%), 780 (75%), 794 (21%), 805 [$C_{60}C(CO)$-$(CO_2H)^+$, 24%], 824 (20%), 919 (12%), 921 (11%), 935 ($MH^+$, 5%), and 937 (7%); FT-IR (KBr) $\nu_{max}$ 3429 (vs, water peak), 2976 (m, −C−H stretching), 2924 (m, −C−H stretching), 2849 (m), 1741 (vs, malonyl ester −C═O), 1633 (m), 1454 (s, antisymmetric deformations of $-CH_3$), 1427 (m), 1392 (m), 1367 (s, symmetric deformations of $CH_3$), 1273 (vs), 1253 (vs, asymmetric stretching of −C−C(═O)−O−), 1155 (vs, −C−O−*t*-Bu stretching and C($C_{60}$)−C-C(═O)− deformations), 1113 (m), 1059 (w), 1031 (w), 846 (m), 805 (w), 733 (m), 703 (m), 578 (m), 552 (m), and 526 (vs, a characteristic band of $C_{60}$ monoadduct) $cm^{-1}$; UV−vis ($CHCl_3$, cutoff at 245 nm, $1.0 \times 10^{-5}$ M) $\lambda_{max}$ 257 and 323 (shoulder band) nm; $^1H$ NMR (500 MHz, $CDCl_3$, ppm) δ 1.70 (s, 18H); $^{13}C$ NMR (500 MHz, $CDCl_3$, ppm) δ 162.28 (−C═O), 145.79, 145.36, 145.26, 145.18, 144.82, 144.72, 144.56, 143.93, 143.17, 143.15, 143.05, 143.03, 142.30, 141.96, 140.95, 139.00, 84.42, and 72.26, consistent with the structure of **3**.

**Synthesis of 4-Hydroxy-[*N*,*N*′,*N*,*N*,*N*,*N*-hexapropylhexa-(aminoethyl)butanamide, $C_3N_6C_3OH$ 5.** To a solution of $BF_3{\cdot}Et_2O$ (1.98 g, 13.7 mmol) in the anhydrous dichloromethane was added


dx.doi.org/10.1021/jm3000664 | J. Med. Chem. 2012, 55, 4274−4285

triethylamine (1.60 g, 15.8 mmol, predistilled), and the mixture was stirred at 0 °C for a period of 30 min. In a separate flask, *N,N′,N,N,N,N*-hexapropylhexa(aminoethyl)amine, $N_5C_3NH_2$ (1.87 g, 3.9 mmol), and γ-butyrolactone (0.40 g, 4.6 mmol) were dissolved in dichloromethane (10 mL) and added to the above solution. Temperature of the mixture was slowly increased to 25 °C and kept at this temperature overnight. The reaction was quenched by the addition of cold aqueous sodium carbonate (10%). The organic layer was then washed sequentially with aqueous sodium carbonate (10%) and water and subsequently dried over sodium sulfate. After removal of the solvent, the crude product was purified by column chromatography (alumina TLC) using $CHCl_3$–$CH_3OH$ (9.5:0.5, v/v) as the eluent to give a viscous light yellow liquid of 4-hydroxy-[*N,N′,N,N,N,N*-hexapropylhexa(aminoethyl)butanamide $C_3N_6C_3OH$ **5** in 60.0% yield (1.32 g). Spectroscopic data of the compound **5**: FT-IR (KBr) $\nu_{max}$ 3304 (s, −O−H), 2957 (vs, −C−H stretching), 2933 (vs, −C−H stretching), 2872 (vs), 2807 (vs), 1650 (vs, amide carbonyl −C═O), 1555 (s), 1540 (s), 1459 (s), 1381 (m), 1189 (m, −C−C(═O)−NH− and −C(C═O)−NH−C− stretchings), 1077 (s, −C−O− stretching), and 749 (w) $cm^{-1}$; $^1H$ NMR (500 MHz, $CDCl_3$, ppm) δ 3.66 (t, 2H, methylene protons of −C**H**$_2$−OH), 3.27 (t, 2H, methylene protons of −C**H**$_2$−$NH_2$), 2.68−2.32 (br, 32H, amine *N*-attached −C**H**$_2$− protons of ethyleneamino moiety), 1.83 (m, 2H, methylene protons of −CO−$CH_2$−C**H**$_2$−$CH_2$−OH), 1.44 (m, 12H, $CH_3$−C**H**$_2$−$CH_2$−N−), and 0.86 (m, 18H, C**H**$_3$−$CH_2$−$CH_2$−N−); $^{13}C$ NMR (500 MHz, $CDCl_3$, ppm) δ 173.62 (amide −NH−**C**═O), 62.14, 57.45, 57.37, 57.00, 56.94, 56.93, 56.89, 56.84, 56.82, 56.77, 52.93, 52.63, 52.48, 52.43, 52.34, 51.74, 37.70, 34.19, 28.56, 20.44, 20.36, 20.34, 20.30, 20.20, 19.89, 12.12 (4C), and 12.05 (2C).

**Synthesis of Bis(20-oxo-4,7,10,13,16-pentapropyl-4,7,10,13,16,19-hexaazatricosan-23-yl)[70]fullerenyl Malonate, Protonated Quaternary Ammonium Trifluoroacetate Salt, $C_{70}$[>M($C_3N_6^+C_3H$)$_2$] 7.** The compound $C_{70}$[>M($C_3N_6^+C_3H$)$_2$] **7** was synthesized by a transesterification reaction with the following procedure. To a solution of $C_{70}$[>M(*t*-Bu)$_2$] **4** (0.15 g, 0.14 mmol) in 1,2-dichloroethane was added $C_3N_6C_3OH$ **5** (0.23 g, 0.40 mmol) and trifluoroacetic acid (1.0 g, 8.8 mmol). The solution was heated under reflux for a period of 3.0 days until no $C_{70}$[>M(*t*-Bu)$_2$] was detected on an analytical TLC plate ($SiO_2$ with toluene as the eluent). Upon completion of the reaction, the mixture was washed with ice-cold aqueous potassium carbonate and water briefly, dried over sodium sulfate, followed by solvent evaporation to give a brown solid. The excessive $C_3N_6C_3OH$ was removed by several ethyl acetate washings. The product was then quaternized by the addition of trifluoroacetic acid to afford bis(20-oxo-4,7,10,13,16-pentapropyl-4,7,10,13,16,19-hexaazatricosan-23-yl)[60]fullerenyl malonate, protonated quaternary ammonium trifluoroacetate salt, $C_{70}$[>M($C_3N_6^+C_3H$)$_2$] **7**, in a yield of 71% (0.32 g). Spectroscopic data of the compound **7**: FT-IR (KBr) $\nu_{max}$ 3441 (vs, water peak), 3006 (m), 2968 (s, −C−H stretching), 2929 (s, −C−H stretching), 2871 (m), 2852 (m), 1727 (m, malonyl ester −C═O), 1648 (vs, amide carbonyl −C═O), 1551 (w), 1453 (vs, antisymmetric deformations of $-CH_3$), 1433 (s), 1387 (m), 1372 (m, symmetric deformations of $CH_3$), 1280 (w), 1252 (w), 1197 (w), 1155 (s, C($C_{60}$)−C−C(═O)− deformations and −C−O−C− stretching), 1095 (m), 1034 (m), 946 (s), 880 (w), 840 (w), 796 (s, $C_{70}$), 750 (s), 708 (w), 658 (w), 625 (w), 582 (s, $C_{70}$), 536 (s, $C_{70}$), and 469 (br) $cm^{-1}$; UV−vis (DMF, cutoff at 268 nm, $1.0 \times 10^{-5}$ M) $\lambda_{max}$ 327−563 nm (a broad shoulder band); $^1H$ NMR (500 MHz, $CDCl_3$–$CS_2$–DMF-$d_7$, ppm) δ 4.0−4.15 (m, br, 4H, carboxylated methylene protons −C(═O)−O−C**H**$_2$−), 3.32−4.0 (m, br, 56H, protonated quaternary ammonium ethylene protons −$N^+$−C**H**$_2$−), 3.11−3.20 (m, br, 8H, including −C(═O)−NH−C**H**$_2$−), 2.28 (m, 4H, −CO−$CH_2$−C**H**$_2$−$CH_2$−OH), 1.76 (m, 24H, $CH_3$−C**H**$_2$−$CH_2$−N−), and 0.97 (m, 36H, C**H**$_3$−$CH_2$−$CH_2$−N−); $^{13}C$ NMR (500 MHz, $CDCl_3$–$CS_2$–DMSO-$d_6$, ppm) 170.45 (amide −NH−**C**═O), 165.50 (ester −O−**C**═O), 155.81, 155.65, 155.51, 154.24, 153.64, 150.31, 150.28, 149.83, 149.65, 149.37, 149.11, 148.85, 148.84, 147.53, 147.49, 147.41, 147.36, 147.15, 146.83, 146.74, 146.72, 146.63, 146.61, 146.55, 146.54, 146.50, 145.88, 145.80, 145.62, 145.55, 145.18, 145.15, 144.59, 144.29, 144.18, 144.10, 144.04, 143.99, 143.44, 142.51, 142.25, 142.19, 142.08, 142.00, 141.89, 141.53, 141.45, 141.21, 140.82, 140.75, 140.31, 140.19, 139.73, 139.03, 138.67, 138.60, 137.83, 137.16, 136.02, 132.08, 131.86, 130.96, 130.92, 130.27, 129.05, 128.96 (2C), and 128.88 for the fullerenyl $sp^2$ carbons, indicating a $C_1$ symmetry for the fullerene cage. Signals of aliphatic carbons of the polycationic arm moiety were low because of the high incompatibility of this moiety under the current solvent mixture used.

A similar procedure was applied for the preparation of bis(20-oxo-4,7,10,13,16-pentapropyl-4,7,10,13,16,19-hexaazatricosan-23-yl)[60]-fullerenyl malonate, protonated quaternary ammonium trifluoroacetate salt, $C_{60}$[>M($C_3N_6^+C_3H$)$_2$] **6**, in 65.2% yield. Spectroscopic data: FT-IR (KBr) $\nu_{max}$ 3436 (vs), 2957 (s, −C−H stretching), 2927 (s, −C−H stretching), 2868 (m), 2843 (m), 2809 (m), 1714 (m, malonyl ester −C═O), 1622 (vs, amide carbonyl −C═O), 1523 (w), 1456 (s, antisymmetric deformations of $-CH_3$), 1428 (m), 1361 (m, symmetric deformations of $CH_3$), 1322 (w), 1184 (m), 1152 (m, C($C_{60}$)−C−C(═O)− deformations and −C−O−C− stretching), 1046 (m), 740 (s), 706 (s), 573 (m), and 526 (vs, a characteristic band of $C_{60}$ monoadduct) $cm^{-1}$; UV−vis ($CHCl_3$, cutoff at 245 nm, $1.0 \times 10^{-5}$ M) $\lambda_{max}$ 285 nm (shoulder peak); $^1H$ NMR (500 MHz, $CDCl_3$–$CS_2$–DMF-$d_7$, ppm) δ 4.0−4.25 (m, br, 4H, carboxylated methylene protons −C(═O)−O−C**H**$_2$−), 3.32−4.10 (m, br, 56H, protonated quaternary ammonium ethylene protons −$N^+$−C**H**$_2$−), 3.11−3.20 (m, br, 8H, including −C(═O)−NH−C**H**$_2$−), 2.34 (m, 4H, −CO−$CH_2$−C**H**$_2$−$CH_2$−OH), 1.68 (m, 24H, $CH_3$−C**H**$_2$−$CH_2$−N−), and 0.88 (m, 36H, C**H**$_3$−$CH_2$−$CH_2$−N−); $^{13}C$ NMR (500 MHz, $CDCl_3$–$CS_2$–DMF-$d_7$, ppm) 147.99 (2C), 145.79 (2C), 144.82 (2C), 144.36 (2C), 144.18 (2C), 144.14 (2C), 144.10 (2C), 144.05, 143.74, 143.66 (2C), 143.64 (2C), 143.55 (2C), 143.46 (2C), 143.28 (2C), 142.96 (2C), 142.88, 142.73 (2C), 142.25 (2C), 142.12 (4C), 141.97 (2C), 141.93 (2C), 141.82 (2C), 141.55 (2C), 141.23 (2C), 141.13 (2C), 140.07, 139.80 (2C), 139.48 (2C), 136.74 (2C), and 135.46 (2C) for the fullerenyl $sp^2$ carbons, indicating a $C_2$ symmetry for the fullerene cage. Signals of aliphatic carbons of the polycationic arm moiety were low because of high incompatibility of this moiety under the current solvent mixture used.

**Synthesis of Decacationic Bis(20-oxo-4,7,10,13,16-pentapropyl-4,7,10,13,16,19-hexaazatricosan-23-yl)[70]fullerenyl Malonate, Methyl Quaternary Ammonium Iodide Salt, $C_{70}$[>M-($C_3N_6^+C_3$)$_2$] 2.** A suspension solution of **7** (0.20 g, 0.063 mmol) in chloroform (20 mL) was added to potassium carbonate/DMF solution (20 mL), and the mixture was subsequently stirred for a period of 1.0 h. To this brown solution was added iodomethane (12 mL, excess, addition in portions over the full reaction period). The reaction mixture was kept at 45 °C for 3.0 days. At the end of reaction, excessive iodomethane and solvent were removed via evaporation and the excess $K_2CO_3$ was removed by quick wash using water to give the product $C_{70}$[>M($C_3N_6^+C_3$)$_2$] **2** in a yield of 91.0% (0.20 g). Spectroscopic data: MALDI−TOF−MS (sinapic acid as the matrix, rel intensity) *m/z* 819 (40%), 841 ($C_{70}H^+$, 100%), 855 ($C_{70}$−$CH_3^+$, 15%), 1355, 1584, 1654, 1682, 1753, 2043, 2079, and 3340 (M − $I^-$); *m/z* 841 ($C_{70}H^+$, 80%), 855 ($C_{70}$−$CH_3^+$, 100%), 913 (40%), 1036 (15%), 1124 (15%), 1344 (15%), 1369 (15%), 1440 (10%), 1577 (15%), and 1794 (15%); FT-IR (KBr) $\nu_{max}$ 3437 (vs, water peak), 3006 (m), 2957 (m, −C−H stretching), 2923 (s, −C−H stretching), 2852 (m), 1735 (m, malonyl ester −C═O), 1642 (vs, amide carbonyl −C═O), 1465 (vs), 1427 (m), 1385 (m), 1317 (w), 1243 (w), 1209 (w), 1157 (w), 1111 (w), 1043 (m), 943 (m), 794 (m, $C_{70}$), 757 (w), 723 (w), 671 (m, $C_{70}$), 618 (m), 579 (s, $C_{70}$), 530 (s, $C_{70}$), 501 (m), and 459 (m) $cm^{-1}$; UV−vis (DMF, cutoff at 268 nm, $1.0 \times 10^{-5}$ M) $\lambda_{max}$ 327−563 nm (a broad shoulder band); $^1H$ NMR (500 MHz, DMSO-$d_6$, ppm) δ 3.82−4.43 (m, br, 36H, carboxylated methylene protons −C(═O)−O−C**H**$_2$− and methylated quaternary ammonium ethylene protons −$N^+$−C**H**$_2$−), 3.10−3.69 (m, br, 32H, methylated quaternary ammonium ethylene protons −$N^+$−C**H**$_2$− and −C(═O)−NH−C**H**$_2$−), 2.22 (m, 4H, −CO−$CH_2$−C**H**$_2$−$CH_2$−OH), 1.58−1.90 (m, 24H, $CH_3$−C**H**$_2$−$CH_2$−N−), and 0.97 (m, 36H, C**H**$_3$−$CH_2$−$CH_2$−N−). Elemental analysis of **2** gave C, 43.90; H, 4.38; N, 5.09; I, 37.35%.C, 54.08; H, 4.53; N, 4.24; I, 29.14%,


dx.doi.org/10.1021/jm3000664 | J. Med. Chem. 2012, 55, 4274−4285

indicating a measured $I/N_q$ (quaternary amine) ratio of 0.97 as the same degree of quaternization on average.

A similar procedure was applied for the preparation of decacationic bis(20-oxo-4,7,10,13,16-pentapropyl-4,7,10,13,16,19-hexaaza-tricosan-23-yl)[60]fullerenyl malonate, methyl quaternary ammonium iodide salt, $C_{60}[>M(C_3N_6^+C_3)_2]$ **1**, in 92.0% yield. Spectroscopic data: MALDI−TOF−MS (sinapic acid as the matrix, rel intensity) $m/z$ 703 (50%), 721 ($C_{60}H^+$, 100%), 759 (20%), 928 (40%), 946 (20%), 1595, 1648, 1682, 1839, 1989, 2039, 2152 (10%), 2359 (10%), 2468, 2626, 2794, 2838, 2852, and 3220 ($M - I^-$); ESI−MS (rel intensity) $m/z$ 630, 720 ($C_{60}$), 871 [$C_{60}$−$C(CO-O-CH{=}CH)_2^+$, 100%], 872, 885, 942, 949, 984, 985, 1043 (30%), 1045, 1067, 1114, 1208, 1210, 1282, 1570 [a group of six peaks, 8%, $M^+ - 10I - 8(CH_2CH_2CH_3) - 4HCH_3 - HN(CH_2CH_2CH_3)_2$, consistent with further fragmentations from the peak of $m/z$ 1760], 1587, 1591, 1608, 1623, 1625, 1741, 1742 (3%), and 1760 [a group of seven peaks, 2%, $MH^+ - 10I - 6(CH_2CH_2CH_3) - 4CH_3$, consistent with a mass of fully decationized **1**, giving evidence of a $C_{60}$ malonate monoadduct with two 4-hydroxyhexa(aminoethyl)butanamide main chains]; FT-IR (KBr) $\nu_{max}$ 3427 (vs, water peak), 2964 (s, −C−H stretching), 2928 (s, −C−H stretching), 2874 (m), 2850 (m), 1752 (w, malonyl ester −C═O), 1711 (w), 1650 (vs, amide carbonyl −C═O), 1457 (vs), 1373 (m), 1320 (w), 1182 (m), 1102 (w), 1080 (m), 1032 (s), 947 (m), 756 (w), 727 (m), 708 (w), 693 (w), 578 (m), and 526 (vs, a characteristic band of $C_{60}$ monoadduct) $cm^{-1}$; UV−vis (DMF, cutoff at 268 nm, $1.0 \times 10^{-5}$ M) $\lambda_{max}$ 323 nm (shoulder peak); $^1H$ NMR (500 MHz, DMSO-$d_6$, ppm) $\delta$ 3.82−4.43 (m, br, 36H, carboxylated methylene protons −C(═O)−O−C**H**$_2$− and methylated quaternary ammonium ethylene protons −$N^+$−C**H**$_2$−), 3.10−3.69 (m, br, 32H, methylated quaternary ammonium ethylene protons −$N^+$−C**H**$_2$− and −C(═O)−NH-C**H**$_2$−), 2.22 (m, 4H, −CO−$CH_2$−C**H**$_2$−$CH_2$−OH), 1.58−1.90 (m, 24H, $CH_3$−C**H**$_2$−$CH_2$−N−), and 0.97 (m, 36H, C**H**$_3$−$CH_2$−$CH_2$−N−). Elemental analysis of **1** giving C, 54.08; H, 4.53; N, 4.24; I, 29.14% indicated a measured $I/N_q$ (quaternary amine) ratio of 0.92 as the same degree of quaternization on average.

**Synthesis of Decacationic Bis(20-oxo-4,7,10,13,16-pentapropyl-4,7,10,13,16,19-hexaazatricosan-23-yl)[70]fullerenyl Malonate, Methyl Quaternary Ammonium Triflouroacetate Salt, $C_{70}[>M(C_3N_6^+C_3)_2]$ 2′.** Ion-exchange reaction of the compound $C_{70}[>M(C_3N_6^+C_3)_2]$ **2** (30 mg, 0.0087 mmol) was carried out in DMF solution by the addition of an excess quantity of aqueous $CF_3COONa$. The mixture was heated at 50 °C and sonicated for a period of 1.0 h. The product was precipitated from the solution upon the addition of methanol. The solids were washed by methanol and diethyl ether. The resulting solids were subjected to a repeated ion-exchange procedure and followed by drying under vacuum to afford the corresponding methyl quaternary ammonium salt $C_{70}[>M(C_3N_6^+C_3)_2]$ **2′** with triflouroacetate anions in a nearly quantitative yield. Spectroscopic data: FT-IR (KBr) $\nu_{max}$ 3436 (vs, water peak), 3006 (m), 2969 (s, −C−H stretching), 2932 (m, −C−H stretching), 2877 (m), 2757 (m), 1726 (m, malonyl ester −C═O), 1640 (s, amide carbonyl −C═O), 1457 (s), 1431 (m), 1332 (w), 1209 (m), 1156 (s), 1086 (m), 1018 (m), 945 (s), 880 (m), 794 (m, $C_{70}$), 754 (w), 673 (m, $C_{70}$), 576 (s, $C_{70}$), 532 (s, $C_{70}$), and 472 (m) $cm^{-1}$; $^1H$ NMR (500 MHz, $CDCl_3$−$CS_2$−DMSO-$d_6$, ppm) $\delta$ 4.09−4.39 (m, br, 36H, carboxylated methylene protons −C(═O)−O−C**H**$_2$− and methylated quaternary ammonium ethylene protons −$N^+$−C**H**$_2$−), 2.86−3.50 (m, br, 32H, methylated quaternary ammonium ethylene protons −$N^+$−C**H**$_2$− and −C(═O)−NH−C**H**$_2$−), 2.12 (m, 4H, −CO−$CH_2$−C**H**$_2$−$CH_2$−OH), 1.45−1.95 (m, 24H, $CH_3$−C**H**$_2$−$CH_2$−N−), and 0.74−1.11 (m, 36H, C**H**$_3$−$CH_2$−$CH_2$−N−); $^{13}C$ NMR (500 MHz, $CDCl_3$−$CS_2$−DMSO-$d_6$, ppm) 170.45 (amide −NH−**C**═O), 155.81, 155.67, 155.50, 154.20, 153.10, 150.31, 149.83, 149.65, 149.37, 149.11, 148.87, 148.84, 148.82, 147.84, 147.64, 147.53, 147.49, 147.41, 147.36, 147.15, 146.83, 146.74, 146.72, 146.63, 146.61, 146.23, 146.21, 146.15, 146.10, 145.88, 145.80, 145.62, 145.55, 145.18, 145.15, 144.59, 144.38, 144.36, 144.34, 144.29, 144.10, 144.04, 143.99, 143.45, 142.51, 142.26, 142.22, 142.21, 142.19, 141.53, 141.45, 141.21, 141.15, 140.82, 140.31, 140.19, 139.73, 137.79, 137.77, 134.97, 134.15, 131.86, 130.96, 130.92, 129.05, 129.00, 128.94, and 128.88 for the fullerenyl $sp^2$ carbons, indicating a $C_1$ symmetry for the fullerene cage. Signals of aliphatic carbons of the polycationic arm moiety were low because of high incompatibility of this moiety under the current solvent mixture used.

A similar procedure was applied for the preparation of decacationic bis(20-oxo-4,7,10,13,16-pentapropyl-4,7,10,13,16,19-hexaazatricosan-23-yl)[60]fullerenyl malonate, methyl quaternary ammonium triflouroacetate salt, $C_{60}[>M(C_3N_6^+C_3)_2]$ **1′**. Spectroscopic data: FT-IR (KBr) $\nu_{max}$ 3448 (vs, water peak), 2970 (s, −C−H stretching), 2924 (s, −C−H stretching), 2877 (m), 2846 (m), 1728 (s, malonyl ester −C═O), 1647 (vs, amide carbonyl −C═O), 1457 (vs), 1393 (w), 1368 (m), 1251 (w), 1213 (m), 1186 (m), 1154 (vs), 1111 (s), 1090 (s), 1019 (m), 944 (m), 752 (m), 613 (m), 576 (m), and 526 (vs, a characteristic band of $C_{60}$ monoadduct) $cm^{-1}$; $^1H$ NMR (500 MHz, $CDCl_3$−$CS_2$−DMSO-$d_6$, ppm) $\delta$ 4.09−4.39 (m, br, 36H, carboxylated methylene protons −C(═O)−O−C**H**$_2$− and methylated quaternary ammonium ethylene protons −$N^+$−C**H**$_2$−), 2.86−3.50 (m, br, 32H, methylated quaternary ammonium ethylene protons −$N^+$−C**H**$_2$− and −C(═O)−NH−C**H**$_2$−), 2.12 (m, 4H, −CO−$CH_2$−C**H**$_2$-$CH_2$−OH), 1.45−1.95 (m, 24H, $CH_3$−C**H**$_2$−$CH_2$−N−), and 0.74−1.11 (m, 36H, C**H**$_3$−$CH_2$−$CH_2$−N−); $^{13}C$ NMR (500 MHz, $CDCl_3$−$CS_2$−DMSO-$d_6$, ppm) 147.09 (2C), 144.37 (2C), 143.85, 143.81 (2C), 143.69 (2C), 143.67, 143.61 (2C), 143.28 (2C), 143.23 (2C), 143.14 (2C), 143.03 (2C), 142.65, 142.35 (2C), 142.22 (2C), 141.89, 141.60 (4C), 141.48 (2C), 141.45 (2C), 140.70 (2C), 139.52 (2C), 139.38 (2C), 139.16 (2C), 138.77 (2C), 138.53 (2C), 138.23 (2C), 137.76 (2C), 137.33 (2C), 136.68 (2C), 136.67 (2C), and 136.58 (2C) for the fullerenyl $sp^2$ carbons, indicating a $C_2$ symmetry for the fullerene cage. Signals of aliphatic carbons of the polycationic arm moiety were low because of high incompatibility of this moiety under the current solvent mixture used.

**Cell Culture.** A human cervical cancer cell line HeLa[37] was obtained from ATCC (Manassas, VA). The cells were cultured in RPMI medium with L-glutamine and $NaHCO_3$ supplemented with 10% heat-inactivated fetal bovine serum, penicillin (100 U/mL) (Sigma, St. Louis, MO) at 37 °C in 5% $CO_2$ humidified atmosphere in 75 $cm^2$ flasks (Falcon, Invitrogen, Carlsbad, CA). When the cells reached 80% confluence, they were washed with phosphate buffered saline (PBS) and harvested with 2.0 mL of 0.25% trypsin−EDTA solution (Sigma). Cells were then centrifuged and counted in trypan blue to ensure viability and plated at a density of 5000/well in flat-bottom 96-well plates (Fisher Scientific, Pittsburgh, PA).

**Bacterial Culture.** *Staphylococcus aureus* 8325-4 and *Escherichia coli* K12 (both wild type) were obtained from ATCC. Planktonic bacterial cells were cultured in brain−heart infusion (BHI) broth with aeration at 37 °C to stationary phase overnight and refreshed to mid-log growth phase for 2.0 h the next day. Cell numbers were estimated by measuring the optical density (OD) at 600 nm [OD of 0.5 = $10^8$ cells/mL].

**Light Source for Bioexperiments.** We used a white (400−700 nm) broad-band light source (Lumacare, Newport Beach, CA) set to deliver a spot of 5.0 cm diameter at an irradiance of 100 mW/$cm^2$. The power was measured with a power meter (model DMM 199 with 201 standard head, Coherent, Santa Clara, CA).

**PDT of Bacteria.** Mid-log phase cells were collected through centrifugation (1000$g$) for 5 min and then suspended in PBS. A cell suspension consisting of $10^8$ cells/mL for bacteria was incubated with fullerene for 30 min at room temperature in the dark. Then 500 $\mu$L aliquots of cell suspension were transferred to a 48-well plate and fullerene derivative, **1** or **2**, was added (up to 10 $\mu$M for *S. aureus* and up to 80 $\mu$M for *E. coli*) from a DMA stock solution prepared at 2.0 mM. The highest concentration (for 80 $\mu$M fullerene) of DMA used was 4%, and this did not cause any toxicity to the cells. Cells were illuminated at room temperature for 16.6 min to deliver 100 J/$cm^2$. At the completion of the illumination period, 100 $\mu$L aliquots were removed from illuminated and nonilluminated wells (cells incubated with fullerene but kept in 48-well plates covered with aluminum foil at room temperature for the duration of the illumination were used as control) and serially diluted 10-fold in PBS to give dilutions of $10^{-1}$−$10^{-6}$ times the original concentrations, and 10 $\mu$L aliquots of each of the dilutions were streaked horizontally on square BHI plates by the


dx.doi.org/10.1021/jm3000664 | J. Med. Chem. 2012, 55, 4274−4285

method of Jett and colleagues.[38] Plates were streaked in triplicate and incubated for 24 h at 37 °C in the dark to allow colony formation. Controls groups included cells that were not treated with fullerene or light and cells treated with light but not with fullerene. Survival fractions (SF) were routinely expressed as ratios of CFU of microbial cells treated with light and fullerene or treated with fullerene in the dark to CFU of microbes treated with neither.

**PDT of Cancer Cells.** After cells had grown for 24 h, dilutions of fullerene derivatives were prepared in complete RPMI medium containing 10% serum, penicillin (100 U/mL), and streptomycin (100 μg/mL) and added to the cells at 2.0 μM for an additional incubation of 24 h. The highest DMA concentration in the medium did not exceed 0.1%. The medium was replaced with fresh complete medium, and white light (400−700 nm with a fluence of 0, 10, 20, 40, and 80 J/cm$^2$) was delivered at an irradiance of 100 mW/cm$^2$. The light spot covered four wells, which were considered as one experimental group illuminated at the same time. Control groups were as follows: no treatment, light alone, and fullerene alone (at the same dilution used for PDT experiments). Following PDT treatment the cells were returned to the incubator overnight and a 4.0 h MTT assay was carried out the next day and read at 562 nm using a microplate spectrophotometer (Spectra Max 340 PC, Molecular Devices, Sunnyvale, CA). Each experiment was repeated 3 times.

**Fluorescence Probe Assay Procedures.** The 96-well black-sided plates were used for fluorescence probe experiments. SOG (in methanol) or HPF (in DMF as provided by Invitrogen, Ltd. with a final concentration of 5.0 μM) was added to 5.0 μM $C_{60}$[>M-($C_3N_6^+C_3$)$_2$] **1** or $C_{70}$[>M($C_3N_6^+C_3$)$_2$] **2** in phosphate buffered saline (PBS) solution (200 μL) per well. Fluorescence spectrometry (SpectraMax M5 plate reader, Molecular Devices, Sunnyvale, CA) used excitation and emission at 504 and 525 nm for SOG and 490 and 515 nm for HPF, respectively. Increasing fluence (J/cm$^2$) was delivered using a blue LED light source (415 ± 15 nm, Clear-U, Photomedex, Montgomeryville, PA) at an irradiance of 20 mW/cm$^2$. Each time after an incremental fluence was delivered, the fluorescence was measured.

**Statistics.** Values are the mean of three separate experiments, and bars presented in the graphs are standard errors of the mean (SEM). Differences between mean values were statistically analyzed by one-way ANOVA in Microsoft Excel, and $p < 0.05$ was considered significant.

## ■ ASSOCIATED CONTENT

### Ⓢ Supporting Information

Additional details of spectroscopic data for the structural characterization of all compounds given in Scheme 1. This material is available free of charge via the Internet at http://pubs.acs.org.

## ■ AUTHOR INFORMATION


### Corresponding Author

*For M.R.H.: phone, +1 617-726-6182; e-mail, hamblin@helix.mgh.harvard.edu. For L.Y.C.: phone, +1 978-934-3663; e-mail, Long_Chiang@uml.edu.


### Notes

The authors declare no competing financial interest.

## ■ ACKNOWLEDGMENTS

We thank the financial support of National Institutes of Health (NIH) under Grant 1R01CA137108.

## ■ REFERENCES


(1) Dolmans, D. E.; Fukumura, D.; Jain, R. K. Photodynamic therapy for cancer. *Nat. Rev.* **2003**, *3*, 380−387.

(2) Hamblin, M. R.; Hasan, T. Photodynamic therapy: a new antimicrobial approach to infectious disease? *Photochem. Photobiol. Sci.* **2004**, *3*, 436−450.

(3) O'Riordan, K.; Akilov, O. E.; Hasan, T. The potential for photodynamic therapy in the treatment of localized infections. *Photodiagn. Photodyn. Ther.* **2005**, *2*, 247−262.

(4) Silva, J. N.; Filipe, P.; Maziere, P.; Maziere, J. C.; Freitas, J. P.; Cine de Castro, J. P.; Santus, R. Photodynamic therapy: dermatology and ophthalmology as main fields of current applications in clinic. *Bio-Med. Mater. Eng.* **2006**, *16*, S147−S154.

(5) Castano, A. P.; Demidova, T. N.; Hamblin, M. R. Mechanisms in photodynamic therapy: part one: photosensitizers, photochemistry and cellular localization. *Photodiagn. Photodyn. Ther.* **2004**, *1*, 279−293.

(6) Castano, A. P.; Demidova, T. N.; Hamblin, M. R. Mechanisms in photodynamic therapy: part two: cellular signalling, cell metabolism and modes of cell death. *Photodiagn. Photodyn. Ther.* **2005**, *2*, 1−23.

(7) Livermore, D. M. The threat from the pink corner. *Ann. Med.* **2003**, *35*, 226−234.

(8) Tang, H. M.; Hamblin, M. R.; Yow, C. M. A comparative in vitro photoinactivation study of clinical isolates of multidrug-resistant pathogens. *J. Infect. Chemother.* **2007**, *13*, 87−91.

(9) Mroz, P.; Tegos, G. P.; Gali, H.; Wharton, T.; Sarna, T.; Hamblin, M. R. Photodynamic therapy with fullerenes. *Photochem. Photobiol. Sci.* **2007**, *6*, 1139−1149.

(10) Navarre, W. W.; Schneewind, O. Surface proteins of Gram-positive bacteria and mechanisms of their targeting to the cell wall envelope. *Microbiol. Mol. Biol. Rev.* **1999**, *63*, 174−229.

(11) Scott, J. R.; Barnett, T. C. Surface proteins of Gram-positive bacteria and how they get there. *Annu. Rev. Microbiol.* **2006**, *60*, 397−423.

(12) Kell, A. J.; Stewart, G.; Ryan, S.; Peytavi, R.; Boissinot, M.; Huletsky, A.; Bergeron, M. G.; Simard, B. Vancomycin-modified nanoparticles for efficient targeting and preconcentration of Gram-positive and Gram-negative bacteria. *ACS Nano* **2008**, *2*, 1777−1788.

(13) Demidova, T. N.; Hamblin, M. R. Photodynamic therapy targeted to pathogens. *Int. J. Immunopathol. Pharmacol.* **2004**, *17*, 245−254.

(14) Bingel, C. Cyclopropylation of fullerenes. *Chem. Ber.* **1993**, *126*, 1957−1959.

(15) Birkett, P. R.; Avent, A. G.; Darwish, A. D.; Kroto, H. W.; Taylor, R.; Walton, D. R. M. Formation and characterisation of $C_{70}Cl_{10}$. *J. Chem. Soc., Chem. Commun.* **1995**, 683−685.

(16) Thilgen, C.; Hermann, A.; Diederich, F. The covalent chemistry of higher fullerenes: $C_{70}$ and beyond. *Angew. Chem., Int. Ed. Engl.* **1997**, *36*, 2268−2280.

(17) Thilgen, C.; Diederich, F. The higher fullerenes: covalent chemistry and chirality. *Top. Curr. Chem.* **1999**, *199*, 136−171.

(18) Sawamura, M.; Nagahama, N.; Toganoh, M.; Hackler, U. E.; Isobe, H.; Nakamura, E.; Zhou, S.; Chu, B. *Chem. Lett.* **2000**, 1098−1099.

(19) Brettreich, M.; Burghardi, S.; Bottcher, C.; Bayerl, T.; Bayerl, S.; Hirsch, A. *Angew. Chem., Int. Ed.* **2000**, *39*, 1845−1848.

(20) Zhou, S.; Burger, C.; Chu, B.; Sawamura, M.; Nagahama, N.; Toganoh, M.; Hackler, U. E.; Isobe, H.; Nakamura, E. *Science* **2001**, *291*, 1944−1947.

(21) Foley, S.; Berberan-Santos, M. N.; Fedorov, A.; McGarvey, D. J.; Santos, C.; Gigante, B. Photophysical properties of pseudo-dihydro derivatves of $C_{70}$. *J. Phys. Chem. A* **1999**, *103*, 8173−8178.

(22) Brites, M. J.; Santos, C.; Nascimento, S.; Gigante, B.; Luftmann, H.; Fedorov, A.; Berberan-Santos, M. N. Synthesis and fluorescence properties of [60] and [70]fullerene-coumarin dyads: Efficient dipole−dipole resonance energy trasfer from coumarin to fullerene. *New J. Chem.* **2006**, *30*, 1036−1045.

(23) Guldi, D. M.; Prato, M. Excited-state properties of $C_{60}$ fullerene derivatives. *Acc. Chem. Res.* **2000**, *33*, 695−703.

(24) Yamakoshi, Y.; Umezawa, N.; Ryu, A.; Arakane, K.; Miyata, N.; Goda, Y.; Masumizu, T.; Nagano, T. Active oxygen species generated from photoexcited fullerene ($C_{60}$) as potential medicines: $O_2^{-\bullet}$ versus $^1O_2$. *J. Am. Chem. Soc.* **2003**, *125*, 12803−12809.

(25) Kuznetsova, N. A.; Gretsova, N. S.; Yuzhakova, O. A.; Negrimovskii, V. M.; Kaliya, O. L.; Luk'yanets, E. A. New reagents

for determination of quantum efficiency of singlet oxygen generation in aquesou media. *Russ. J. Gen. Chem.* **2001**, *71*, 36−41.
(26) Raga's, X.; Jimenez-Banzo, A.; Sanchez-Garcia, D.; Batllori, X.; Nonell, S. Singlet oxygen photosensitisation by the fluorescent probe Singlet Oxygen Sensor Greens. *Chem. Commun.* **2009**, 2920−2922.
(27) Setsukinai, K.-I.; Urano, Y.; Kakinuma, K.; Majima, H. J.; Nagano, T. Development of novel fluorescence probes that can reliably detect reactive oxygen species and distinguish specific species. *J. Biol. Chem.* **2003**, *278*, 3170−3175.
(28) Gupta, A. K.; Rohatgi-Mukherjee, K. K. Solvent effect on photosensitized oxidation of iodide ion by anthracene sulphonates. *Photochem. Photobiol.* **1978**, *27*, 539−543.
(29) Huang, L.; Dai, T.; Hamblin, M. R. Antimicrobial photodynamic inactivation and photodynamic therapy for infections. *Methods Mol. Biol.* **2010**, *635*, 155−173.
(30) Huang, L.; Xuan, Y.; Koide, Y.; Zhiyentayev, T.; Tanaka, M.; Hamblin, M. R. Type 1 and type 2 mechanisms of antimicrobial photodynamic therapy: an in vitro study on Gram-negative and Gram-positive bacteria. *Laser Surg. Med.*, in press.
(31) Valduga, G.; Bertoloni, G.; Reddi, E.; Jori, G. Effect of extracellularly generated singlet oxygen on Gram-positive and Gram-negative bacteria. *J. Photochem. Photobiol., B* **1993**, *21*, 81−86.
(32) Dahl, T. A.; Midden, W. R.; Hartman, P. E. Comparison of killing of Gram-negative and Gram-positive bacteria by pure singlet oxygen. *J. Bacteriol.* **1989**, *171*, 2188−2194.
(33) Lu, Z.; Dai, T.; Huang, L.; Kurup, D. B.; Tegos, G. P.; Jahnke, A.; Wharton, T.; Hamblin, M. R. Photodynamic therapy with a cationic functionalized fullerene rescues mice from fatal wound infections. *Nanomedicine (London, U.K.)* **2010**, *5*, 1525−1533.
(34) Mroz, P.; Xia, Y.; Asanuma, D.; Konopko, A.; Zhiyentayev, T.; Huang, Y. Y.; Sharma, S. K.; Dai, T.; Khan, U. J.; Wharton, T.; Hamblin, M. R. Intraperitoneal photodynamic therapy mediated by a fullerene in a mouse model of abdominal dissemination of colon adenocarcinoma. *Nanomedicine* **2011**, *7*, 965−974.
(35) Sharma, S. K.; Chiang, L. Y.; Hamblin, M. R. Photodynamic therapy with fullerenes in vivo: reality or a dream? *Nanomedicine (London, U.K.)* **2011**, *6*, 1813−1825.
(36) Martinez, G. R.; Garcia, F.; Catalani, L. H.; Cadet, J.; Oliveira, M. C. B.; Ronsein, G. E.; Miyamoto, S.; Medeiros, M. H. G.; Di Mascio, P. Synthesis of a hydrophilic and non-ionic anthracene derivative, the *N,N'*-di(2,3-dihydroxypropyl)-9,10-anthracenedipropanamide as a chemical trap for singlet molecular oxygen detection in biological systems. *Tetrahedron* **2006**, *62*, 10762−10770.
(37) Perry, V. P. Cultivation of large cultures of HeLa cells in horse serum. *Science* **1955**, *121*, 805.
(38) Jett, B. D.; Hatter, K. L.; Huycke, M. M.; Gilmore, M. S. Simplified agar plate method for quantifying viable bacteria. *BioTechniques* **1997**, *23*, 648−650.